Research Article

Received: 22 August 2023 Revised: 22 November 2023 Accepted article published: 21 February 2024 Published online in Wiley Online Library:

(wileyonlinelibrary.com) DOI 10.1002/jsfa.13401

Effect of fibers on starch structural changes during hydrothermal treatment: multiscale analyses, and evaluation of dilution effects on starch digestibility

Özge Güven and İlkay Şensoy*

Abstract

BACKGROUND: Dietary fibers (DFs) may influence the structural, nutritional and techno-functional properties of starch within food systems. Moreover, DFs have favorable effects on the digestive system and potentially a lower glycemic index. These potential benefits may change depending on DF type. Starch processed in the presence of soluble and insoluble fibers can undergo different structural and functional changes, and the present study investigated the effects of short-chain and long-chain inulin and cellulose on the structural and digestive properties of wheat starch.

RESULTS: The combined use of differential scanning calorimetry, Fourier transform infrared spectroscopy (FTIR) and X-ray diffraction (XRD) provided insights into the structural changes in starch and inulin at different levels. Short-chain and long-chain inulin had higher water retention capacity and a potential to limit starch gelatinization. The FTIR results revealed an interaction between starch and inulin. Scanning electron microscopy analysis showed morphological changes in starch and inulin after the hydrothermal treatment. Cellulose fiber was not affected by the hydrothermal treatment and had no influence on starch behavior. The structural differences observed through XRD, FTIR and scanning electron microscopy analyses between starch with and without inulin fibers did not significantly impact starch digestibility, except for the dilution effect caused by adding DFs.

CONCLUSION: The present study highlights the importance of utilizing different analytical tools to assess changes in food samples at different scales. Although short-chain and long-chain inulin could potentially limit starch gelatinization, the duration of the heat treatment (90 °C for 10 min) was sufficient to ensure complete starch gelatinization. The dilution effect caused by adding fibers was the primary reason for the effect on starch digestibility.

Keywords: thermal processing; gelatinization; carbohydrate digestion; supramolecular structure; molecular order

INTRODUCTION

Dietary fibers (DFs) have many health benefits, such as the prevention of cancer and cardiovascular and digestive systems diseases, and protection against obesity and diabetes.[1-4] DFs affect starch metabolism, and they have been reported to decrease glycemic index[1,5] and there is increasing interest in investigating the relationship between DFs and glycemic index.

Inulin is a water-soluble polysaccharide found in several edible fruit and vegetables. Commercial inulin has different degrees of polymerization (DP), and inulin can be in a crystalline or amorphous phase.[6] An amorphous state may increase upon processing inulin using different techniques.[7] Although inulin is assumed to affect blood glucose levels, it is unclear whether it has an increasing or decreasing effect since studies have shown contradicting results.[8] Cellulose is a water-insoluble DF found in sea mosses, plants and some bacteria, which produce cellulose, and it makes the cell walls of those organisms along with hemicellulose and lignin.[9] Partially crystalline cellulose is embedded in the amorphous region of hemicellulose and lignin.[9,10] Cellulose, in its natural form, is not generally used as a food additive, although it is abundant in many plant-based foods. Thus, it may exist in many food systems composed of starch, and its effect on starch structure and digestibility has not been well-covered in the literature.

Various studies suggest a diverse range of results on the effect of soluble and insoluble DFs on starch digestibility, making it hard to make a common conclusion. For example, according to a study on the glycemic index of fiber-enriched cakes by Kyung *et al.*,[4]

* *Correspondence to: İ Şensoy, Department of Food Engineering, Middle East Technical University, 06800 Ankara, Turkey. E-mail: isensoy@metu.edu.tr*

Department of Food Engineering, Middle East Technical University, Ankara, Turkey

insoluble DFs reduce the predicted glycemic index more effectively than soluble DFs. On the other hand, it was also reported that *in vitro* starch digestibility (or glucose release) behavior was correlated with only total DF content regardless of whether the majority is soluble or insoluble fiber.[11] Building upon these highlights, the present study aimed to comprehensively investigate the changes in starch structure and digestibility that occur after hydrothermal processes in the presence and absence inulin and cellulose fibers to compare the effects of those fibers as examples of soluble and insoluble fibers on structural, nutri-functional, and techno-functional properties.

MATERIALS AND METHODS

Materials

Materials used in the experiments were commercial wheat starch (Tito, Smart Kimya, İzmir, Turkey), short-chain inulin (Orafti®GR; BENEO GmbH, Mannheim, Germany), long-chain inulin (Orafti®HPX; BENEO GmbH) and cellulose (Jelucel®PF300; JELU-WERK J. Ehrler GmbH & Co. KG, Rosenberg, Germany). Short chain inulin had maximum 10 g glucose + fructose + sucrose in 100 g of inulin on dry basis. Average degree of polymerization was higher than 10. Long chain inulin had maximum 0.5 g of glucose + fructose + sucrose in 100 g of inulin on a dry basis. Average degree of polymerization was higher than 23.

Sample preparation

Samples were prepared according to the experimental design given in Table 1.

Raw samples

Starch and DF mixtures were prepared to contain 50:50 (g:g) starch:DF on dry basis. Then, distilled water was added to the mixtures to obtain 1:1, 1:2, and 1:4 (g:mL) dry matter-to-water ratios. The native starch and DF samples were prepared similarly, using the same water ratios.

Heat-processed samples

Samples containing 30 g of dry matter, prepared at room temperature, were taken into sealable 8 × 10-cm polypropylene bags. The bags were placed horizontally between two aluminum plates and cooked in a water bath at 90 °C for 10 min. After cooling for about 30 min at room temperature, they were frozen at −80 °C for 1 day before being freeze-dried for 24 ± 1 h at around 0.03 mbar in a freeze drier (Alpha 2–4 LD Plus; Martin Christ, Osterode am Harz, Germany). Dried samples were finely ground and passed through a sieve (1 mm; Fritsch, Idar-Oberstein, Germany) for further analysis.

Differential scanning calorimetry (DSC)

Samples (raw and cooked) containing around 5 mg dry matter were placed into aluminum pans and equilibrated at room temperature (approximately 24 °C) for at least 3 h. The scanning process was executed between 30 °C and 110 °C at 10 °C min^{-1} heating rate[12] with a differential scanning calorimeter (DSC 4000; Perkin Elmer, Hopkinton, MA, USA) using an empty pan as reference system.

X-ray diffraction (XRD)

XRD analyses were conducted according to the method described by Chen *et al.*[13] with some modifications. The diffractograms of mixtures and the pure fiber samples were obtained by Ultima-IV (Rigaku, Tokyo, Japan) and Miniflex (Rigaku, Tokyo, Japan) X-ray diffractometers, respectively, at 40 kV and 30 mA. Diffractograms of samples were obtained at 1 °/min scanning rate between 4° and 40° (2θ). The measurements were conducted in three replicates. All diffractograms were plotted with Origin software (OriginPro 2023; OriginLab, Northampton, MA, USA), and all data sets were normalized between 0 and 1. For each sample, a representative diffractogram was drawn for qualitative analysis using the average intensity values from three replicates corresponding to each angle 2θ.

Crystallinity calculation by two-phase method

The two-phase approach, as described in Lopez-Rubio et al.,[14] states that a baseline (amorphous baseline) cutting the upper portion of crystal peaks separates the crystalline and amorphous regions of XRD diffractogram. Origin software (OriginPro 2023; OriginLab) was used to determine the amorphous baseline. The total area between the XRD plot and amorphous baseline, crystalline area (A_C), and the area under the amorphous baseline (AA) were calculated using the same software. Relative crystallinity by two-phase approach RC_{TP} was calculated according to:

$$RC_{TP}\% = \frac{A_C}{A_C + A_A} \times 100 \quad (1)$$

Crystallinity calculation by crystal-defect method

The crystal-defect method is based on fitting the obtained diffractograms into the Gaussian function to determine the peak parameters: peak center, peak area, and full-width-at-half-maximum.[14] The diffractograms were fitted into the Gaussian function using Origin software (OriginLab) for each sample. The Levenberg–Marquardt algorithm was used to find the final coefficient values that minimize chi-squared. The iterative fitting procedure terminated when the chi-squared value decreased by less than 0.00001 between two successive iterations. The relative crystallinity by crystal-defect method (RC_{CD}) was calculated using the sum

Table 1. Experimental design parameters of the model systems

Factors	Levels		
Dietary fiber (DF) type	Short-chain Inulin	Long-chain Inulin	Cellulose
Wheat starch:DF ratio (g:g, dry basis)	100:0 (Control)	50:50	
Dry matter:water ratio (g:mL)	Low (1:1)	Medium (1:2)	High (1:4)

Note: Dry matter:water ratio represents the water content during cooking at 90 °C for 10 min.

of the areas of the fitted peaks (A_{FP}) and the area of the amorphous halo (A_{AH}) according to:

$$RC_{CD}\% = \frac{A_{FP}}{A_{FP}+A_{AH}} \times 100 \quad (2)$$

Fourier transform infrared spectroscopy (FTIR)

FTIR analyses with some modifications were performed based on the methods described elsewhere.[15] Raw and cooked samples were scanned between the wavelengths 4000 cm^{-1} and 600 cm^{-1}, at a resolution of 4 cm^{-1}, with 256 scans by an FTIR spectrometer (IR-Affinity-1; Shimadzu, Kyoto, Japan) in an attenuated total reflectance (ATR) mode using a diamond ATR crystal. FTIR-ATR spectra of the samples were plotted using Origin software (OriginLab). The analyses were conducted out in three replicates. The spectrum of each sample was plotted using the wavelength *vs*. intensity data, and all data sets were normalized between 0 and 1. A representative spectrum was drawn for each sample by averaging the three intensity values (replicates) corresponding to each wavelength value.

Scanning electron microscopy (SEM)

The SEM images were taken by 400F Field Emission instrument (QUANTA, Holland) at METU Central Laboratory (Çankaya, Turkey) as described elsewhere.[16] Samples were placed on spots and covered by 6 nm Au—Pd before they were scanned at an acceleration rate of 20 kV.

In vitro starch digestion

Digestion analyses of the model systems were conducted according to Englyst *et al*.,[17] with some modifications described below. Total glucose (TG) determination was based on Englyst *et al*.[18]

Preparation of enzyme solutions

Solution 1 (S1). A total of 0.6 g of guar (G4129; Sigma-Aldrich, St Louis, MO, USA) was wetted with 1 mL of ethanol and dissolved in 120 mL of 0.05 M HCl. In the original method[17] the solution contains pepsin enzyme; however, in the present study, the addition of pepsin was skipped because the samples used contained no protein.

Solution 2 (S2). In three 50-mL tubes, 3 g of pancreatin (8 × USP from porcine pancreas; P-7545; Sigma-Aldrich) was weighed and mixed with 20 mL of $CaCl_2$. A magnetic bar was placed in each tube, and then the tubes were mixed by magnetic stirring for 10 min and occasionally vortex-mixed. The tubes were centrifuged at 1500 × *g* for 10 min at room temperature (approximately 24 °C). From each tube, 17 mL of supernatant was transferred to a beaker and mixed to have 51 mL of solution. Then, 4 mL of amyloglucosidase (≥260 U mL^{-1}; A7095; Sigma-Aldrich) and 2 mL of invertase (10684722; Thermo Fisher Scientific, Waltham, MA, USA) were added to the combined solution. The final solution was mixed by using a magnetic stirrer. This solution was used within 1 h after it was prepared.

Carbohydrate hydrolysis

Heat-processed samples were analyzed after thermal processing and cooling at room temperature for 30 min. In 50-mL tubes, samples containing about 500 mg of available carbohydrates were weighed. Five mL of saturated benzoic acid solution was added to wet the samples. Then, 10 mL of S1 was added to each tube and incubated at 37 °C for 30 min. After the incubation with S1, 5 mL of sodium acetate buffer (0.5 M) was added to all tubes. The pH value of the blank tube was checked, and assured that it varied between 5.2 and 5.35. Five glass balls were added to each tube to provide mechanical disruption, and 5 mL of S2 was added. Tubes were immediately capped and the content was mixed. This time was recorded as 0th min. Then the tubes were placed horizontally in a shaking water bath (JSSB-30T; JSR, Gongju-City, Korea) parallel to the direction of movement. A total of 0.2 mL of sample was transferred from each tube into 8 mL of methanol at 20 min and 120 min to determine the hydrolysis extent. Glucose contents in the tubes were determined using a glucose oxidase-peroxidase assay kit (GOPOD, K-GLUC; Megazyme International Ireland Ltd, Bray, Ireland).

Determination of total glucose

After the carbohydrate digestion procedure, the tubes were vortex-mixed and placed in a boiling water bath for 30 min. At the end of 30 min, the tubes were vortex-mixed and placed in an ice-water bath. In each tube, 10 mL of KOH solution (7 M) was added, mixed by shaking and placed in a shaking ice-water bath parallel to the direction of movement for 30 min. Then, 1 mL of sample was taken from each tube and mixed with 10 mL acetic acid solution (0.5 M, plus 4 mL L^{-1} of 1 M $CaCl_2$ solution). In total, 0.2 mL of previously diluted amyloglucosidase (A7095; Sigma-Aldrich) solution (1 mL:7 mL) was added to each tube. The tubes were vortex-mixed and placed in a 70 °C water bath for 30 min. At the end of 30 min, tubes were left to cool to room temperature and completed to 50 mL by distilled water. The content of the tubes was directly analyzed by a glucose oxidase-peroxidase assay kit (GOPOD, K-GLUC; Megazyme International Ireland Ltd).

Determination of free glucose

Samples containing approximately 500 mg of available carbohydrates were weighed into 50-mL tubes. A total of 5 mL of saturated benzoic acid solution was added to wet the samples. In total, 20 mL of water and 0.25 mL of 1 M sodium acetate were added. The dispersed sample was vortex mixed, and the tubes were placed in a boiling water bath for 30 min. The tubes were taken from the water bath, vortex mixed, and cooled down. At 37 °C, 0.2 mL of invertase (10684722; Thermo Fisher Scientific) was added to each tube and placed in a shaking water bath at 37 °C for 30 min. Finally, tubes were vortex mixed, and 1 mL of sample from each tube was mixed with 2 mL of methanol. Glucose contents in the tubes were determined by a glucose oxidase-peroxidase assay kit (GOPOD, K-GLUC; Megazyme International Ireland Ltd).

Calculation of starch fractions

Total starch (TS), rapidly digestible starch (RDS), slowly digestible starch (SDS) and undigestible starch (US) fractions were calculated using:

$$TS\,(g) = (TG - FG) \times 0.9$$
$$RDS\,(g) = (G20 - FG) \times 0.9$$
$$SDS\,(g) = (G120 - G20) \times 0.9$$
$$US\,(g) = (TG - G120) \times 0.9$$

where FG and TG represent free and total glucose (g), and G20 and G120 represent glucose (g) released at the 20 min and 120 min, respectively.

The results were expressed as RDS/SW, SDS/SW and US/SW ratios (g kg^{-1}) based on dry sample weight (SW), and RDS/TS, SDS/TS and US/TS ratios (g kg^{-1}) based on the total starch (TS).

Statistical analysis

One-way analysis of variance (ANOVA) followed by Tukey's post-hoc tests was performed to determine the statistical difference between means when the normal distribution and homogeneity of variance assumptions were met. In the case of a violation of variance homogeneity, ANOVA was followed by Dunnet's T3 test. In the case of a violation of normality, the Kruskal–Wallis test (followed by non-parametric ANOVA multiple comparison tests) was used. $P < 0.05$ was considered statistically significant. SPSS (IBM Corp. Armonk, NY, USA) was used for the analyses.

RESULTS AND DISCUSSION

Changes in thermal transition properties

Thermal transition parameters of wheat starch with and without the DFs were summarized in Table 2. The enthalpy data was presented in two formats: g^{-1} starch and g^{-1} sample. The starch gelatinization enthalpy at the lowest water concentration (1:1) was low. At the same water ratio (1:1), no transition peak was seen for the short-chain inulin (inulinSC) and long-chain inulin (inulinLC)-added samples. Both inulin and starch have a high affinity to water molecules, so there was a competition for water between inulin and starch.[19] On the other hand, cellulose-added samples revealed comparable transition enthalpy values, 1.97 ± 0.51 J g^{-1} starch (Table 2) with starch. As a water-insoluble DF, cellulose did not significantly affect the thermal properties of starch (Table 2). The enthalpy value, 0.99 ± 0.26 J g^{-1} sample, revealed the dilution and confirmed no competition because one-half of the sample was diluted by cellulose (Table 2).

At higher water ratios (1:2 and 1:4), only the inulinLC-added samples showed lower transition enthalpies (J g^{-1} starch) compared to starch (Table 2). In the DSC thermogram (data not shown), InulinSC demonstrated a transition enthalpy at temperatures lower than starch, with some overlap. Thus, transition enthalpies (J g^{-1} starch) for the starch–inulinSC mixtures could reflect the energy uptake by both inulinSC and starch, masking the limiting effect on gelatinization. It could be stated that inulinSC and inulinLC inhibited the gelatinization at low (1:1) water concentrations. They also limited the gelatinization to some degree at higher water concentrations. The increase in gelatinization peak temperatures at 1:2 and 1:4 water ratios for inulinSC and inulinLC-added samples indicates the delay in gelatinization. Cellulose, on the other hand, as a water-insoluble DF, did not significantly affect the thermal properties of wheat starch.

Wheat starch samples with or without DFs were expected to be gelatinized entirely after being heated at 90 °C for 10 min at the studied water ratios (1:1, 1:2 and 1:4). DSC observations of cooked samples (90 °C for 10 min) at the lowest (1:1) water ratio confirmed these expectations. There was no peak around the gelatinization temperature on the thermograms for the cooked starch with or without DFs (data not shown), demonstrating that starch was completely gelatinized after cooking.

Changes in nanostructure and crystallinity by XRD

Figure 1 presents the XRD patterns of raw and cooked wheat starch with and without DFs, whereas Fig. 2 displays the XRD patterns of raw and cooked DFs. These figures allow for assessing structural changes resulting from interactions between starch and DFs, without interfering with DF self-interactions. Starch showed an XRD pattern with a main unresolved diffraction doublet at around 17–18° and single peaks at around 15°, 20° and 23° (Fig. 1A), which is the typical A-type crystalline structure of starch.[20,21]

Diffraction peaks of wheat starch disappeared after cooking, except for some residual peaks observed in the samples cooked at the lowest water ratio (1:1), indicating some residual crystallinity (Fig. 1A). Interestingly, despite DSC analysis showed complete starch gelatinization after cooking (90 °C for 10 min), residual crystallinity was still evident in XRD diffractograms of the starch samples cooked at the low water ratio (1:1).

The XRD diffractogram of the raw starch–inulinSC mixture showed the typical peaks of the A-type starch crystalline structure above the signals of the inulinSC, but not as clearly defined peaks as seen for the raw starch (Fig. 1B). The amorphous pattern of the

Table 2. Thermal transition properties of wheat starch both with and without fibers at different water contents, determined by differential scanning calorimetry (DSC)

Dry matter:water (g:mL)		Δ H (J g^{-1} starch)	Δ H (J g^{-1} sample)	Onset temperature (°C)	Peak temperature (°C)	End temperature (°C)
1:1	Starch	2.58 ± 0.29 a	2.58 ± 0.29	62.20 ± 0.40 a	67.40 ± 0.17 a	73.02 ± 0.21 a
	Starch–inulinSC	No peak	No peak	No peak	No peak	No peak
	Starch–inulinLC	No peak	No peak	No peak	No peak	No peak
	Starch–cellulose	1.97 ± 0.51 a	0.99 ± 0.26	63.15 ± 0.56 a	67.40 ± 0.29 a	71.56 ± 0.73 b
1:2	Starch	14.28 ± 0.45 a	14.28 ± 0.45	62.38 ± 0.33 c	68.41 ± 0.18 c	78.13 ± 0.23 b
	Starch–inulinSC	12.84 ± 0.17 a	6.42 ± 0.08 a	69.44 ± 0.72 a	74.86 ± 0.66 a	81.73 ± 1.00 a
	Starch–inulinLC	6.74 ± 0.61 b	3.37 ± 0.31 b	66.46 ± 0.28 b	71.80 ± 0.27 b	76.70 ± 0.34 b
	Starch–cellulose	14.66 ± 2.17 a	7.33 ± 1.09 a	63.08 ± 0.14 c	68.55 ± 0.09 c	74.63 ± 0.55 c
1:4	Starch	15.64 ± 1.14 a	15.64 ± 1.14	63.51 ± 0.07 b	69.32 ± 0.18 bc	75.97 ± 0.61 ab
	Starch–inulinSC	16.27 ± 3.02 a	8.13 ± 1.51 a	65.43 ± 0.78 a	71.13 ± 0.89 a	77.27 ± 0.65 a
	Starch–inulinLC	7.22 ± 0.74 b	3.61 ± 0.37 b	65.88 ± 0.41 a	70.62 ± 0.40 ab	76.71 ± 1.45 a
	Starch–cellulose	12.88 ± 1.79 a	6.44 ± 0.89 a	63.36 ± 0.37 b	68.79 ± 0.38 c	74.15 ± 0.70 b

Note: Results are the mean ± SD ($n = 3$). Significantly different onset, peak, end temperature, and ΔH values are followed by different lowercase letters ($P \leq 0.05$) in each water level group in each column.

Journal of The Science of Food and Agriculture published by John Wiley & Sons Ltd on behalf of Society of Chemical Industry.

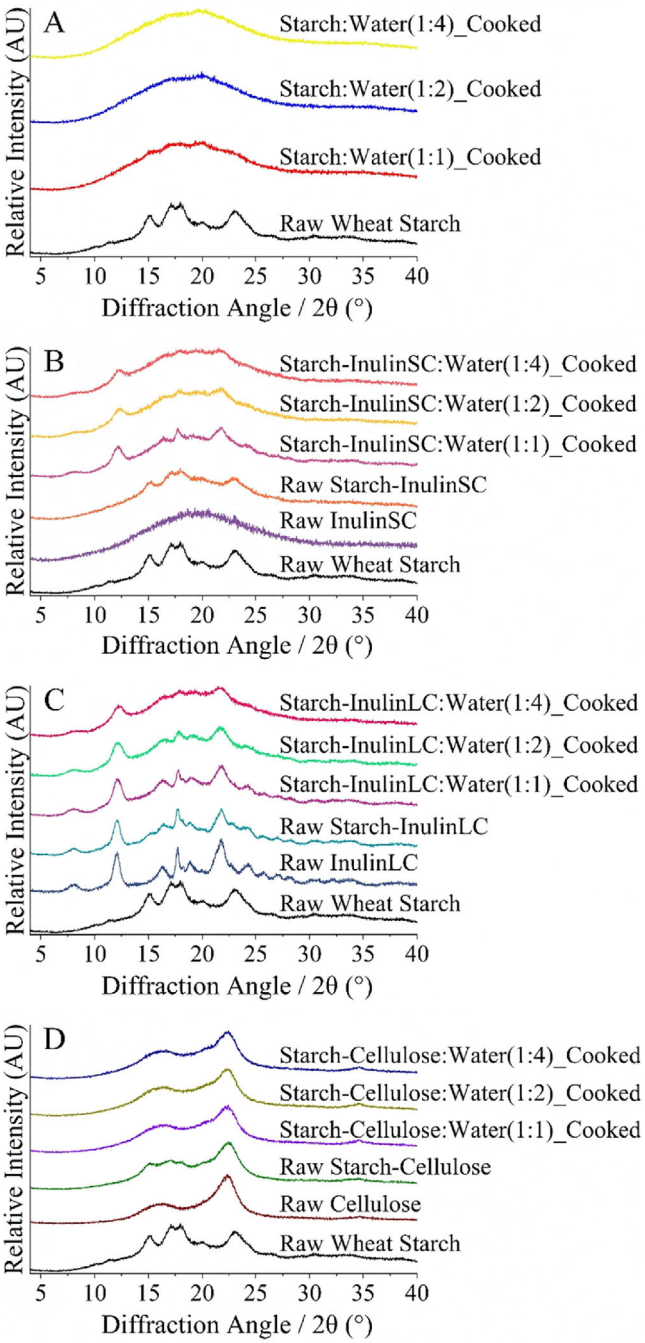

Figure 1. XRD patterns of wheat starch both with and without fibers, in raw state and following hydrothermal treatment at different dry matter-water ratios. (A) raw and cooked wheat starches, (B) raw and cooked starch-short chain inulin mixtures, (C) raw and cooked starch-long chain inulin mixtures and (D) raw and cooked starch–cellulose mixtures.

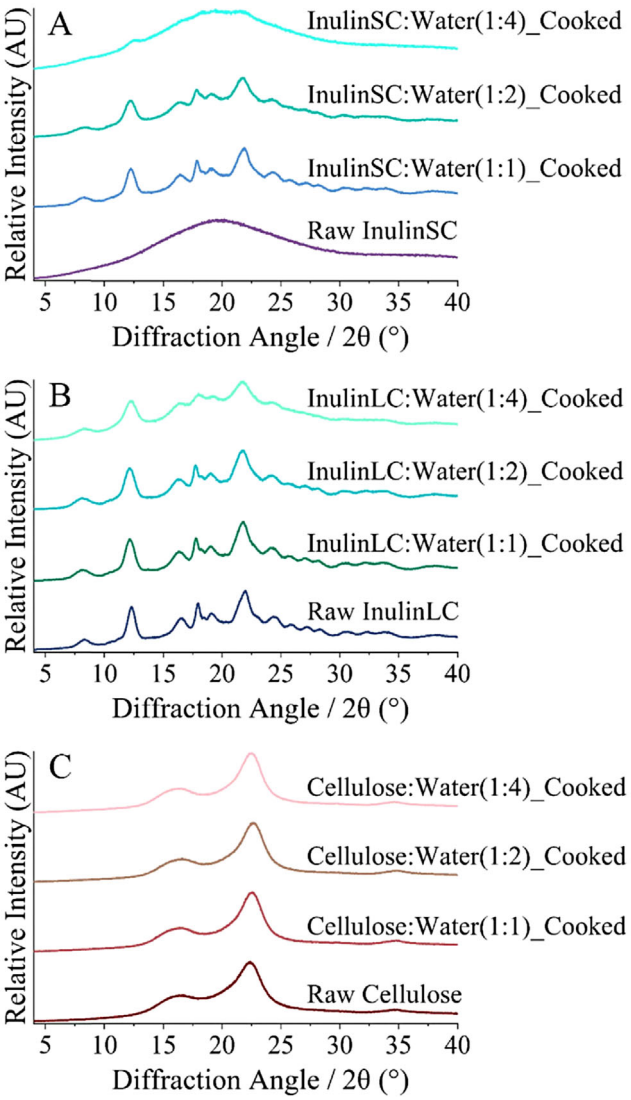

Figure 2. XRD patterns of pure dietary fibers in raw state and following hydrothermal treatment at various dry matter-water ratios. (A) raw and cooked short chain inulin, (B) raw and cooked long chain inulin and (C) raw and cooked cellulose.

inulinSC hindered the crystalline pattern of starch. As depicted in Figs 1(B) and 2(A), the XRD pattern of raw inulinSC alone showed a broad, amorphous pattern with a peak at around 20°, which was previously reported.[20] After hydrothermal treatment, some peaks belonging to starch disappeared, indicating the gelatinization of starch, whereas new diffraction peaks at around 8°, 12°, 16–17°, 18°, 22°, and 24° appeared, especially at the 1:1 water ratio (Fig. 1B). These newly formed peaks were also observed in the pure inulinSC after cooking at low water ratios (Fig. 2A). The XRD pattern of inulinSC cooked at 1:1 water ratio showed diffraction peaks at around 8°, 12°, 16–17°, 18°, 19°, 22°, 24°, 26°, 27°, 28°, 30–31°, 32°, 34°, and 38° (Fig. 2A). The XRD pattern of inulinSC cooked at 1:1 ratio resembled that of raw pure inulinLC (Fig. 2B), indicating that the newly formed crystalline structures resulted from aggregation of inulinSC molecules. Similar observations of new diffraction peaks in pasta samples fortified with inulin were previously reported.[20] The intensities of the newly formed peaks in the cooked starch–inulinSC mixture (1:1 water ratio) decreased or disappeared with increasing water concentration (Fig. 1B). The formation of the crystalline structure in pure inulinSC was minimal at the highest cooking water ratio (1:4), where the inulinSC molecules were almost completely solubilized (Fig. 2A).

The XRD pattern of inulinLC displayed a semi-crystalline pattern (Fig. 2). There were distinct peaks at around 8°, 12°, 16°, 17°–18°, 19°, 21°, and 24° with several other small peaks. The raw starch–inulinLC mixtures displayed a combination of raw starch and raw inulinLC XRD patterns, with the starch peaks mostly obscured

Journal of The Science of Food and Agriculture published by John Wiley & Sons Ltd on behalf of Society of Chemical Industry.

by the inulinLC signals (Fig. 1C). Raw inulin with a higher DP was stated to show crystalline diffraction peaks.[20] As DP increases, the semi-crystalline structure of inulin becomes predominant.[22] After hydrothermal treatment, the relative intensities of the peaks of starch–inulinLC mixtures decreased as the water ratio increased, where the pattern was still visible at the highest water ratio (1:4). The slightly visible peak (15°) belonging to A-type starch disappeared after the hydrothermal treatment, whereas the crystal regions attributed to inulinLC also decreased in intensity with increasing water concentration, indicating a transition towards a more amorphous structure (Fig. 1C). Similar observations were made for pure inulinLC samples cooked at the same water ratios (Fig. 2B).

The raw starch–cellulose mixture exhibited peaks of cellulose and the typical A-type polymorph patterns together (Fig. 2D). Raw, pure cellulose showed three prominent diffraction peaks at around 16°, 22° and 34° (Fig. 2C,D) and they were assigned as the characteristic peaks of lignocellulosic materials, which were previously determined at 15.4°, 22.7° and 34.5° by El Halal *et al*.[23] The starch peaks were mostly hidden behind the cellulose responses (Fig. 1D). After heat treatment, the slightly visible starch peaks were lost due to starch gelatinization, whereas no observable change in the cellulose structure was observed. This lack of change in the cellulose nanostructure was consistent when pure cellulose samples were cooked at the same water ratios (Fig. 2C).

The relative crystallinity (RC) values of the samples are presented in Table 3. These values represented the combined crystallinity of the starch and the added DFs in the raw starch-DF mixtures. As determined by both methods, the RC values of the starch samples decreased after cooking (Table 3). However, despite a few small peaks in the XRD diffractograms for the samples cooked at a water ratio of 1:1 (Fig. 1), neither calculation method indicated a statistically significant difference in the RC of the starch samples.

The RC values of the raw starch–inulinSC mixture were lower (24.13 ± 0.61, 22.20 ± 1.12) than that of pure starch (37.15 ± 2.95, 34.04 ± 2.88), as determined by both the two-phase and crystal-defect methods, respectively. This difference in crystallinity could be attributed to the amorphous structure of inulinSC. The crystal-defect method did not reveal any change in the RC values of starch–inulinSC mixtures after cooking. However, according to the two-phase method, the crystallinity of the mixture cooked at a water ratio of 1:1 was higher compared to both the raw mixture and the mixtures cooked at higher water ratios (Table 3). In these samples, although the starch lost its crystalline structure and gelatinized during cooking, the inulinSC component formed aggregates, which were observed as new crystalline peaks, especially at the low water ratio of 1:1 (Fig. 1B). The diffractograms revealed that after the heat treatment intensity of crystalline peaks of starch–inulinLC mixture decreased with increasing water ratio. The RC values of the starch–cellulose mixtures obtained from the two approaches showed different results. The two-phase method indicated a decrease in RC after cooking at a water ratio of 1:1. By contrast, the crystal-defect method did not reveal any significant change in RC after cooking (Table 3). XRD diffractograms of the starch–cellulose mixtures revealed a slight difference between the raw and the mixture cooked at 1:1 water ratio.

The divergent RC values obtained by the two methods highlight the differences in their assumptions and calculation sensitivities (Table 3). The two-phase method assumes the presence of two distinct phases, crystalline and amorphous, not considering the intermediate crystals in the samples.[24,25] However, this assumption is often invalid for polymeric structures like starch and complex or multi-component food systems. In the case of starch-DF mixtures, overlapping diffraction peaks from different phases could have introduced inaccuracies in the results obtained using this method. On the other hand, the crystal-defect method assumes ideal crystal structures in the samples, which may reduce accuracy when determining the crystallinity in samples such as starch with semi-crystalline structures. The crystalline regions of starch are not perfectly ordered or uniform, and they coexist with

Table 3. Relative crystallinity (RC) values of wheat starch both with and without fibers, in raw state and following hydrothermal treatment at different dry matter–water ratios calculated by two approaches using XRD diffractograms: the two-phase method and the crystal-defect method

	Dry matter:water (g:mL)	RC_{TP} % Two-phase	RC_{CD} % Crystal-defect
Starch	–	37.15 ± 2.95 a	34.04 ± 2.88 a
	1:1	17.73 ± 1.03 b	22.93 ± 1.04 b
	1:2	17.93 ± 1.06 b	19.26 ± 0.89 b
	1:4	18.87 ± 0.66 b	19.90 ± 2.45 b
Starch–inulinSC	–	24.13 ± 0.61 b	22.20 ± 1.12 a
	1:1	27.51 ± 1.04 a	23.42 ± 6.06 a
	1:2	22.87 ± 1.48 b	21.08 ± 2.25 a
	1:4	22.42 ± 0.76 b	20.94 ± 3.46 a
Starch–inulinLC	–	38.77 ± 1.62 a	43.97 ± 3.64 a
	1:1	31.99 ± 0.37 ab	25.45 ± 0.86 b
	1:2	27.76 ± 2.19 ab	23.16 ± 1.79 bc
	1:4	24.99 ± 0.38 b	19.68 ± 0.77 c
Starch–cellulose	–	35.65 ± 1.75 a	34.46 ± 0.53 a
	1:1	31.30 ± 0.88 b	37.25 ± 2.38 a
	1:2	32.45 ± 0.74 ab	38.76 ± 2.50 a
	1:4	32.63 ± 1.90 ab	38.26 ± 1.80 a

Note: Results are the mean ± SD ($n = 3$). Significantly different values in the same box for each DF by different lowercase letters ($P \leq 0.05$). The hypen (–) indicates the raw samples.

Journal of The Science of Food and Agriculture published by John Wiley & Sons Ltd on behalf of Society of Chemical Industry.

amorphous regions. This could result in reduced accuracy because the low-quality intermediate crystals represented by the fitted peaks are considered perfect crystalline structures in RC calculations.

Changes in the molecular orders in starch measured by FTIR

The characteristic IR bands of raw starch at 860 cm^{-1}, 929–930 cm^{-1}, 1076 cm^{-1}, 1105 cm^{-1}, 1124 cm^{-1} and 1149 cm^{-1} did not show dramatic changes after hydrothermal treatment of pure starch (Fig. 3A). The most dramatic changes were the decreased relative intensity of the band at 997 cm^{-1} and the increased relative intensity of the band at 1016 cm^{-1} (Fig. 3A). These changes were previously reported as an indication of an increase in the amorphous portion.[26,27]

The decrease of the band at 997 cm^{-1} is related to the loss of intramolecular hydrogen bonds between hydroxyl groups at the C-6 position or the loss of the structure of branched chains formed by hydrogen bonds at the positions of C-6 and C-1 in amylopectin.[28] Hence, the band change at 997 cm^{-1} is accepted as the change in the short-range order of the double helix.[29] The intensity decrease of the band at 997 cm^{-1} and the increasing intensity of the band at 1016 cm^{-1} indicated the increase in the amorphous starch portion.[27] The band at 1043 cm^{-1} is sensitive to the crystalline structure of starch. This band became non-detectable upon hydrothermal processing, which also showed the loss of ordered structure (Fig. 3B).

For raw inulinSC, observed IR bands were 821 cm^{-1}, 867 cm^{-1}, 931 cm^{-1}, 989 cm^{-1}, 1020 cm^{-1}, 1058 cm^{-1} (a shoulder), a hump around 1103 cm^{-1} and 1110 cm^{-1}, and a shoulder at 1161 cm^{-1} (Fig. 3B). For the uncooked starch–inulinSC mixture, the bands at 860 cm^{-1}, 929 cm^{-1}, 997 cm^{-1}, 1012 cm^{-1}, 1043 cm^{-1} (a shoulder), 1076 cm^{-1}, 1103 cm^{-1} and 1147 cm^{-1} were observed (Fig. 3B). Those bands are a mix of bands from starch and inulinSC, with some bands hiding and others shifting. For raw inulinLC, observed IR bands were 817 cm^{-1}, 873 cm^{-1}, 933 cm^{-1}, 985 cm^{-1} and 1026 cm^{-1}, with a hump around 1103 cm^{-1} and 1110 cm^{-1}, and a shoulder at 1161 cm^{-1} (Fig. 3C). For the raw starch–inulinLC mixture, the bands at 860 cm^{-1}, 931 cm^{-1}, 997 cm^{-1}, 1014 cm^{-1}, 1043 cm^{-1} (a shoulder), 1076 cm^{-1} and 1147 cm^{-1} were observed (Fig. 3C). Similarly, those bands are a blend of bands from starch and inulinLC, with some bonds hiding and others shifting as a result of interaction.

Following the hydrothermal treatment, the bands at 997 cm^{-1} for both inulinSC- and inulinLC-added mixtures shifted slightly to the right, whereas the bands at 1012 cm^{-1} for starch- inulinSC and 1014 cm^{-1} for starch-inulinLC mixtures shifted slightly to the left, showing some interaction between starch and the inulin fibers (Fig. 3B,C). The shoulder at 1043 cm^{-1} in the raw mixtures became invisible, similar to pure starch samples, showing a loss of starch crystallinity. The bands at 821 cm^{-1} and 817 cm^{-1} belonging to inulins became visible. The band at 1076 cm^{-1} belonging to starch did not change. The small band at 1103 cm^{-1} related to starch and inulins became invisible after hydrothermal treatment for all water levels. This was also observed for the starch without fiber. This band shows C—O and C—C stretching with some C-O-H contributions,[30] and the band loss shows a change in the modes related to starch structure. Another change that occurred in both starch–inulin mixtures after the hydrothermal treatment was the change of the band at 1147–1149 cm^{-1}, which was a visible peak in raw mixtures and turned into a shoulder after hydrothermal treatment (Fig. 3B,C). This band remained unchanged after hydrothermal starch treatment without DF (Fig. 3B). The band characterizes the coupling of C—O, C—C and O—H bond stretching, bending, and asymmetric stretching of the C-O-C glycosidic bridge in starch, and is related to the interaction of starch with other components through hydrogen bonding.[25,31] The change of this band in starch–inulin systems showed that inulin addition led to a change in those modes after hydrothermal treatment. Both inulinSC and inulinLC had similar short-range order with starch and showed similar interactions with wheat starch.

The raw cellulose showed IR bands at 896 cm^{-1}, 964 cm^{-1} (a shoulder), 987 (valley), 1029 cm^{-1}, 1049 cm^{-1}, 1103 cm^{-1} (valley) and 1161 cm^{-1} (Fig. 3D). For the raw starch–cellulose mixture, the bands at 860 cm^{-1}, 896 cm^{-1}, 999 cm^{-1}, 1016 cm^{-1}, 1047 cm^{-1} (shoulder), 1076 cm^{-1}, 1103 cm^{-1} and 1153 cm^{-1} were observed, indicating a combination of bands coming from both starch and cellulose with some bands shifted (Fig. 3D). The reduction of the relative intensity at the 1047 cm^{-1} band position for the starch–cellulose mixtures heated at low water ratios and the disappearance of the band for the samples heated at higher water ratios showed the loss of crystalline structure with increasing water content. However, most of the changes as a result of the gelatinization of starch were not visible because of the interference of bands originating from cellulose.

FTIR analysis showed that starch gelatinization led to the loss of short-range order for both starch with or without DFs. Investigation of the peaks for pure and mixed samples before and after the treatment showed that, even though wheat starch was completely gelatinized after the hydrothermal treatment, the starch showed some interaction with both types of inulins and did not show much interaction with cellulose fiber.

Morphological changes observed by scanning electron microscopy

Images of the wheat starch and DFs before and after the hydrothermal treatment showed that during the treatment, starch and inulin went through a transition and interaction of inulinSC and inulinLC with gelatinized starch could be seen (Fig. 4E,F). The morphologies of the heat-treated starch–inulinSC (Fig. 4E) and starch–inulinLC (Fig. 4F) mixtures were different from the heat-treated pure starch (Fig. 4A) and starch–cellulose mixtures (Fig. 4G). The smooth and large pores of gelatinized starch could be seen in the cellulose-added blends distinctly but not in starch–inulinSC and starch–inulinLC mixtures (Fig. 4E–G) because both inulins have changed similarly to starch gelatinization. Inulins completely lost their original structure upon hydrothermal treatment and formed an integrated structure during the heating process while cellulose structure stayed unchanged (Fig. 4A–D).

Changes in *in vitro* starch digestion behavior

The results were presented in two forms to examine the impact of dilution on the digestion fractions: the digested fractions were expressed as a percentage of the total dry sample weight (SW), and the fractions were expressed as a percentage of the total measured starch (TS) in the samples. The findings revealed that the cooking increased the rapidly digestible starch (RDS) fractions and decreased the slowly digestible starch (SDS) fractions in all wheat starch samples, regardless of the presence of DFs (Table 4).

The addition of DFs to wheat starch reduced the measured percentage of RDS in the total dry samples, both for cooked and raw samples (Table 4). However, when the digestion fractions were

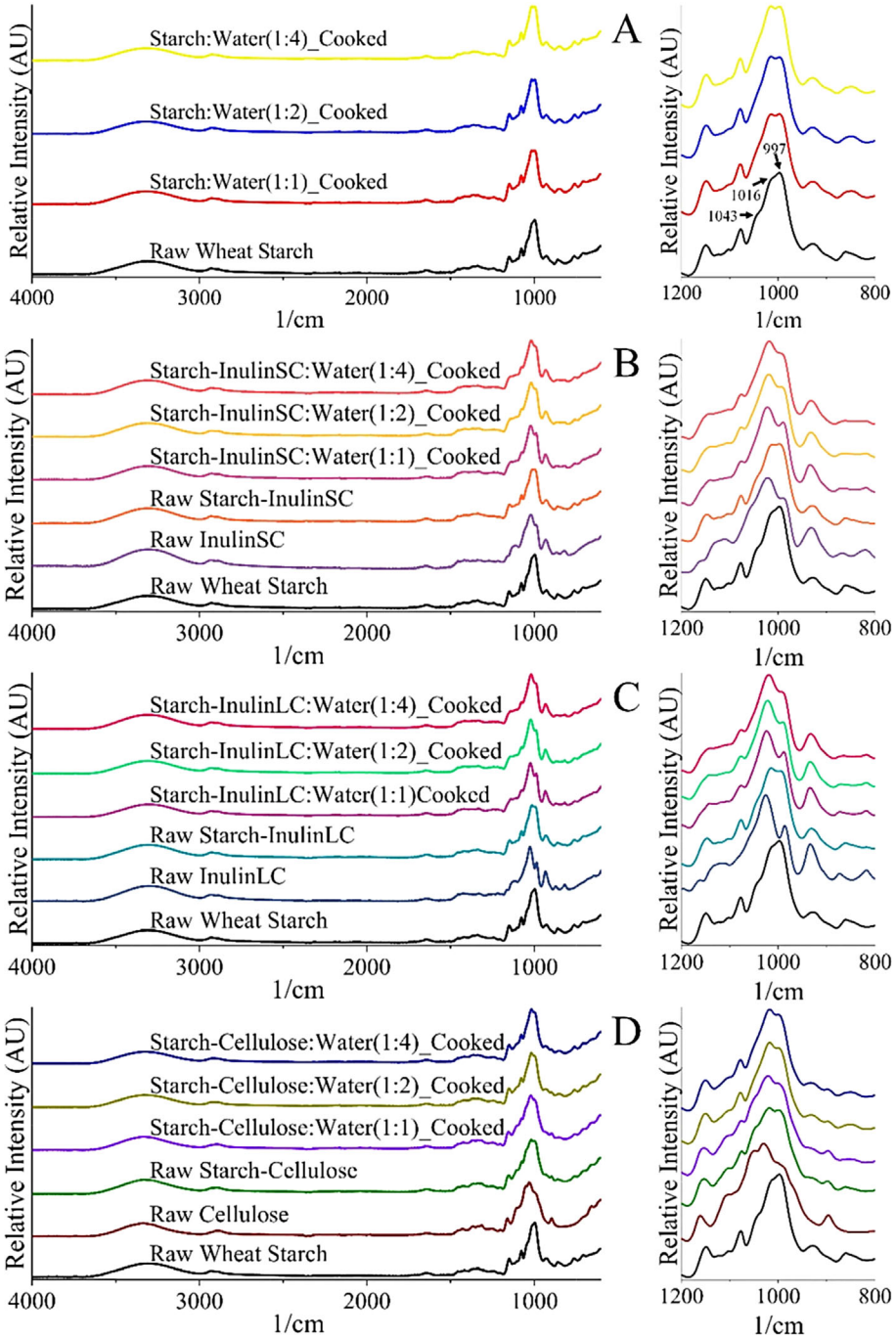

Figure 3. FTIR–ATR spectra of wheat starch both with and without fibers, in raw state and following hydrothermal treatment at different dry matter-water ratios. (A) raw and cooked wheat starches, (B) raw and cooked starch-short chain inulin mixtures, (C) raw and cooked starch-long chain inulin mixtures and (D) raw and cooked starch–cellulose mixtures. Left: Between 600 and 4000 cm^{-1}. Right: Between 800 and 1200 cm^{-1}.

normalized and presented as a percentage of TS in the samples, the data indicated that adding DFs to starch did not result in significant differences in the RDS, SDS or undigestible starch (US) fractions. The effect of dilution was considerable, especially at this level of DF addition.

There were many *in vitro* and *in vivo* studies reporting the effect of soluble and insoluble fibers such as inulin and cellulose fibers on the starch digestibility of products such as breakfast cereals and pasta.[32-41] Non-starch polymers have been shown to indirectly impact starch hydrolysis by increasing the medium viscosity.[42,43] Although the comparison between different processing and analysis methods and the ingredients used can sometimes make it challenging to make direct comparisons, it is generally recommended to incorporate DF to design healthier products. In the context of product development studies, incorporating DFs can be considered a promising approach to reducing the consumption of rapidly digestible starch. Therefore, the utilization of DFs in product formulations holds promise as an effective strategy to improve the nutritional profile and health outcomes associated with starch digestion.

Journal of The Science of Food and Agriculture published by John Wiley & Sons Ltd on behalf of Society of Chemical Industry.

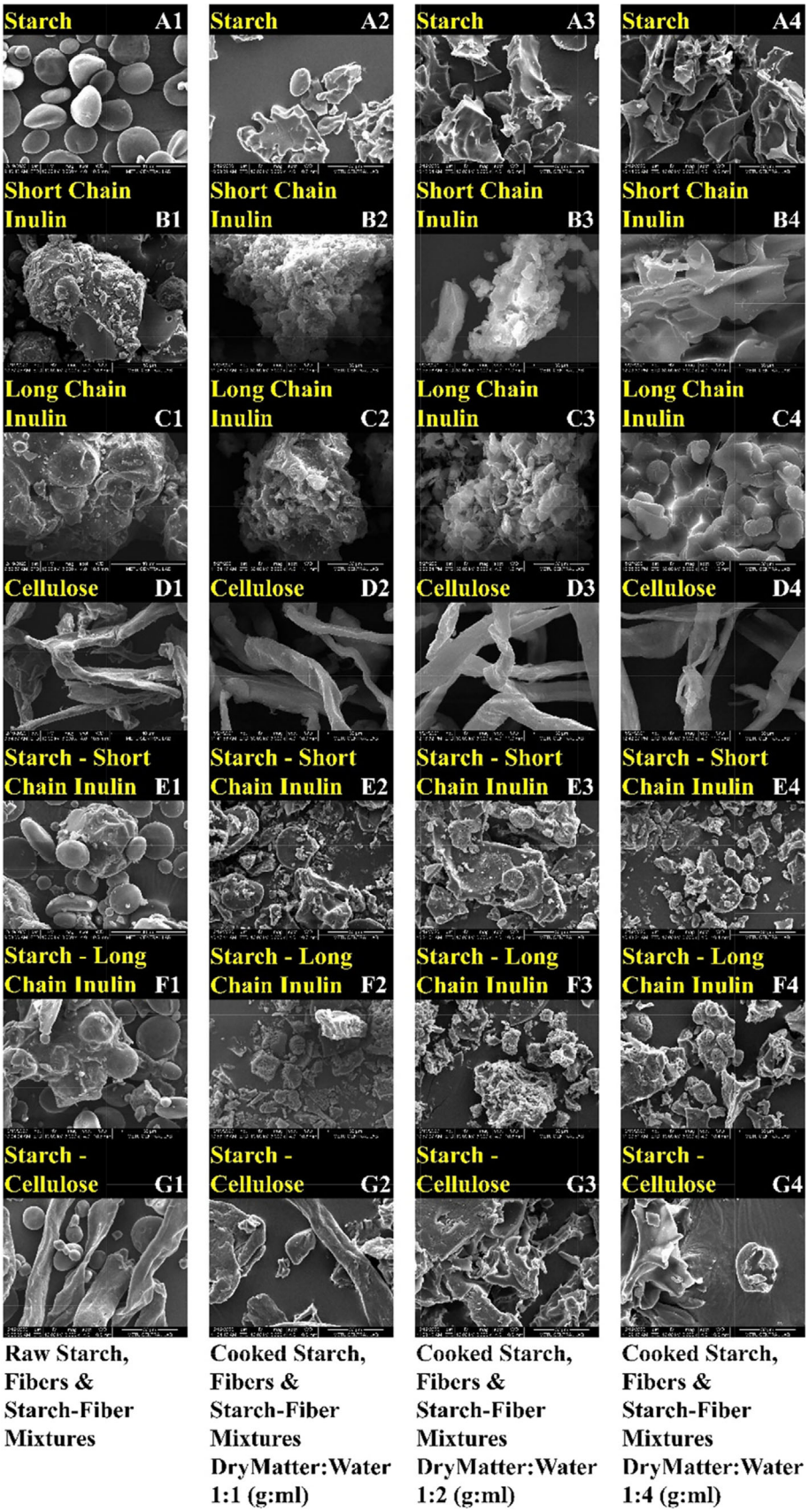

Figure 4. SEM images (×3000 magnification) of wheat starch, dietary fibers, and their mixtures, in raw state and following hydrothermal treatment at different dry matter-water ratios.

Journal of The Science of Food and Agriculture published by John Wiley & Sons Ltd on behalf of Society of Chemical Industry.

Table 4. Digestion fractions of wheat starch, both with and without fibers, per sample weight (SW) and measured total starch (TS), in raw state and following hydrothermal treatment at different dry matter–water ratios

		RDS/SW	SDS/SW	US/SW	RDS/TS	SDS/TS	US/TS
Sample			(g kg^{-1})			(g kg^{-1})	
Raw mixtures	Starch	220 ± 6 a	657 ± 51 a	71 ± 58 a	232 ± 5 a	694 ± 57 a	75 ± 61 b
	Starch–inulinSC	82 ± 14 b	299 ± 12 b	111 ± 27 a	167 ± 31 a	608 ± 38 a	225 ± 48 a
	Starch–inulinLC	96 ± 9 b	304 ± 11 b	74 ± 2 a	203 ± 19 a	641 ± 23 a	155 ± 5 ab
	Starch–cellulose	100 ± 19 b	318 ± 8 b	42 ± 18 a	217 ± 35 a	691 ± 19 a	92 ± 38 ab
Cooked at dry matter:water (1:1)	Starch	787 ± 73 a	84 ± 40 a	86 ± 78 a	821 ± 46 a	87 ± 39 a	92 ± 85 a
	Starch–inulinSC	355 ± 18 b	62 ± 27 a	81 ± 45 a	713 ± 42 a	124 ± 54 a	163 ± 89 a
	Starch–inulinLC	401 ± 28 b	18 ± 8 a	84 ± 21 a	798 ± 58 a	35 ± 16 a	167 ± 42 a
	Starch–cellulose	411 ± 27 b	24 ± 21 a	65 ± 56 a	823 ± 69 a	49 ± 44 a	128 ± 109 a
Cooked at dry matter:water (1:2)	Starch	772 ± 76 a	48 ± 13 a	174 ± 92 a	778 ± 88 a	48 ± 12 a	174 ± 92 a
	Starch–inulinSC	381 ± 37 b	30 ± 7 a	82 ± 52 a	774 ± 96 a	62 ± 16 a	164 ± 102 a
	Starch–inulinLC	386 ± 36 b	19 ± 14 a	72 ± 46 a	810 ± 77 a	41 ± 31 a	150 ± 88 a
	Starch–cellulose	382 ± 35 b	19 ± 3 a	58 ± 21 a	832 ± 53 a	41 ± 7 a	128 ± 47 a
Cooked at dry matter:water (1:4)	Starch	829 ± 68 a	46 ± 19 a	129 ± 43 a	825 ± 52 a	46 ± 20 a	129 ± 45 a
	Starch–inulinSC	412 ± 34 b	33 ± 2 a	63 ± 26 a	811 ± 55 a	65 ± 3 a	124 ± 53 a
	Starch–inulinLC	411 ± 38 b	21 ± 8 a	55 ± 19 a	842 ± 58 a	44 ± 18 a	114 ± 42 a
	Starch–cellulose	390 ± 24 b	36 ± 9 a	63 ± 39 a	798 ± 61 a	73 ± 20 a	129 ± 78 a

Note: Results are the mean ± SD ($n = 3$). Different lowercase letters indicate the significant differences between the samples in each water level group (Raw, 1:1, 1:2 and 1:4) ($P \leq 0.05$).
Abbreviations: RDS, rapidly digestible starch; SDS, slowly digestible starch; US, undigestible starch.

CONCLUSIONS

Thermal analysis indicated a competition between short-chain inulin and long-chain inulin and wheat starch for water. However, the prolonged heat treatment in the study (10 min) was longer than the heating time used in DSC procedure. As a result, this competition did not impact starch gelatinization during cooking.

The DSC, FTIR and XRD data, as well as the SEM images, provided insights into the structural changes in starch and short-chain and long-chain inulin at various levels during hydrothermal treatment. The FTIR results suggested an interaction between starch and both types of inulin during the hydrothermal treatment. The hydrothermal treatment did not affect cellulose fiber and cellulose addition did not impact starch during this process.

It was observed that, although short-chain and long-chain inulin could potentially limit starch gelatinization, the duration of the heat treatment was sufficient to ensure complete starch gelatinization. Furthermore, the structural differences observed through sensitive techniques for starch with and without inulin fibers did not significantly affect starch digestibility, except for the dilution effect caused by adding fibers.

ACKNOWLEDGMENTS

This research was partially supported by Middle East Technical University (Orta Doğu Teknik Üniversitesi) scientific research projects funds (Project numbers: GAP-314-2018-2742 and DKT-314-2018-3617).

CONFLICTS OF INTEREST

The authors declare that they have no conflicts of interest.

DATA AVAILABILITY STATEMENT

The data that support the findings of this study are available from the corresponding author upon reasonable request.

REFERENCES

1 Thebaudin JY, Lefebvre AC, Harrington M and Bourgeois CM, Dietary fibres: nutritional and technological interest. *Trends Food Sci Technol* **8**:41–48 (1997). https://doi.org/10.1016/S0924-2244(97)01007-8.
2 Anderson JW, Baird P, Davis RH, Ferreri S, Knudtson M, Koraym A *et al.*, Health benefits of dietary fiber. *Nutr Rev* **67**:188–205 (2009). https://doi.org/10.1111/j.1753-4887.2009.00189.x.
3 Prosky L, What is fibre? Current controversies. *Trends Food Sci Technol.* **10**:271–275 (1999). https://doi.org/10.1016/S0924-2244(99)00059-X.
4 Kyung I, Young I and Gyu H, International journal of biological macromolecules in vitro starch digestion and cake quality: impact of the ratio of soluble and insoluble dietary fiber. *Int J Biol Macromol.* **63**: 98–103 (2014). https://doi.org/10.1016/j.ijbiomac.2013.10.038.
5 Ng SH, Robert SD, Wan Ahmad WAN and Wan Ishak WR, Incorporation of dietary fibre-rich oyster mushroom (Pleurotus sajor-caju) powder improves postprandial glycaemic response by interfering with starch granule structure and starch digestibility of biscuit. *Food Chem.* **227**:358–368 (2017). https://doi.org/10.1016/j.foodchem.2017.01.108.
6 Romano N, Araujo-Andrade C, Lecot J, Mobili P and Gómez-Zavaglia A, Infrared spectroscopy as an alternative methodology to evaluate the effect of structural features on the physical-chemical properties of inulins. *Food Res Int* **109**:223–231 (2018). https://doi.org/10.1016/j.foodres.2018.04.032.
7 Saavedra-Leos MZ, Leyva-Porras C, Martínez-Guerra E, Pérez-García SA, Aguilar-Martínez JA and Álvarez-Salas C, Physical properties of inulin and inulin-orange juice: physical characterization and technological application. *Carbohydr Polym.* **105**:10–19 (2014). https://doi.org/10.1016/j.carbpol.2013.12.079.
8 Schuchardt JP, Wonik J, Bindrich U, Heinemann M, Kohrs H, Schneider I *et al.*, Glycemic index and microstructure analysis of a newly developed fiber enriched cookie. *Food Funct* **7**:464–474 (2016). https://doi.org/10.1039/C5FO01137J.
9 Hemmati F, Jafari SM and Taheri RA, Optimization of homogenization-sonication technique for the production of cellulose nanocrystals from cotton linter. *Int J Biol Macromol* **137**:374–381 (2019). https://doi.org/10.1016/j.ijbiomac.2019.06.241.
10 Ventura-Cruz S and Tecante A, Extraction and characterization of cellulose nanofibers from rose stems (Rosa spp.). *Carbohydr Polym.* **220**: 53–59 (2019). https://doi.org/10.1016/j.carbpol.2019.05.053.

Journal of The Science of Food and Agriculture published by John Wiley & Sons Ltd on behalf of Society of Chemical Industry.

11 Bae IY, Jun Y, Lee S and Lee HG, Characterization of apple dietary fibers influencing the in vitro starch digestibility of wheat flour gel. *LWT – Food Sci Technol* **65**:158–163 (2016). https://doi.org/10.1016/j.lwt.2015.07.071.

12 Bao JS, Cai YZ and Corke H, Prediction of rice starch quality parameters by near-infrared reflectance spectroscopy. *J Food Sci* **66**:936–939 (2001). https://doi.org/10.1111/j.1365-2621.2001.tb08215.x.

13 Chen L, Ren F, Zhang Z, Tong Q and Rashed MMA, Effect of pullulan on the short-term and long-term retrogradation of rice starch. *Carbohydr Polym.* **115**:415–421 (2015). https://doi.org/10.1016/j.carbpol.2014.09.006.

14 Lopez-Rubio A, Flanagan BM, Gilbert EP and Gidley MJ, A novel approach for calculating starch crystallinity and its correlation with double helix content: a combined XRD and NMR study. *Biopolymers* **89**:761–768 (2008). https://doi.org/10.1002/bip.21005.

15 Ji N, Liu C, Li M, Sun Q and Xiong L, Interaction of cellulose nanocrystals and amylase: its influence on enzyme activity and resistant starch content. *Food Chem.* **2017**:481–487 (2018). https://doi.org/10.1016/j.foodchem.2017.10.130.

16 Caltinoglu C, Tonyalı B and Sensoy I, Effects of tomato pulp addition on the extrudate quality parameters and effects of extrusion on the functional parameters of the extrudates. *Int J Food Sci Technol.* **49**:587–594 (2013). https://doi.org/10.1111/ijfs.12341.

17 Englyst K, Goux A, Meynier A, Quigley M, Englyst H, Brack O *et al.*, Inter-laboratory validation of the starch digestibility method for determination of rapidly digestible and slowly digestible starch. *Food Chem.* **2017**:1183–1189 (2018). https://doi.org/10.1016/j.foodchem.2017.11.037.

18 Englyst KN, Hudson GJ and Englyst HN, Starch analysis in food, in *Encyclopedia of Analytical Chemistry*, 1st edn. John Wiley & Sons, Chichester (2000).

19 Krystyjan M, Ciesielski W, Khachatryan G, Sikora M and Tomasik P, Structure, rheological, textural and thermal properties of potato starch - inulin gels. *LWT – Food Sci Technol.* **60**:131–136 (2015). https://doi.org/10.1016/j.lwt.2014.07.056.

20 Aravind N, Sissons MJ, Fellows CM, Blazek J and Gilbert EP, Effect of inulin soluble dietary fibre addition on technological, sensory, and structural properties of durum wheat spaghetti. *Food Chem* **132**:993–1002 (2012). https://doi.org/10.1016/j.foodchem.2011.11.085.

21 Karwasra BL, Gill BS and Kaur M, Rheological and structural properties of starches from different Indian wheat cultivars and their relationships. *Int J Food Prop* **20**:S1093–S1106 (2017). https://doi.org/10.1080/10942912.2017.1328439.

22 Ronkart SN, Deroanne C, Paquot M, Fougnies C, Lambrechts JC and Blecker CS, Characterization of the physical state of spray-dried inulin. *Food Biophys* **2**:83–92 (2007). https://doi.org/10.1007/s11483-007-9034-7.

23 El Halal SLM, Colussi R, Deon VG, Pinto VZ, Villanova FA, Carreño NLV *et al.*, Films based on oxidized starch and cellulose from barley. *Carbohydr Polym.* **133**:644–653 (2015). https://doi.org/10.1016/j.carbpol.2015.07.024.

24 Ahmed S, Flanagan BM, Zhang B, Dhital S, Junejo SA, Flanagan BM *et al.*, Starch structure and nutritional functionality – Past revelations and future prospects. *Carbohydr Polym* **277**:118837 (2022). https://doi.org/10.1016/j.carbpol.2021.118837.

25 Ma Z and Boye JI, Research advances on structural characterization of resistant starch and its structure-physiological function relationship: a review. *Crit Rev Food Sci Nutr* **58**:1059–1083 (2018). https://doi.org/10.1080/10408398.2016.1230537.

26 Warren FJ, Gidley MJ and Flanagan BM, Infrared spectroscopy as a tool to characterise starch ordered structure - a joint FTIR-ATR, NMR, XRD and DSC study. *Carbohydr Polym.* **139**:35–42 (2016). https://doi.org/10.1016/j.carbpol.2015.11.066.

27 Deeyai P, Suphantharika M, Wongsagonsup R and Dangtip S, Characterization of modified tapioca starch in atmospheric argon plasma under diverse humidity by FTIR spectroscopy. *Chin Phys Lett* **30**:3–6 (2013). https://doi.org/10.1088/0256-307X/30/1/018103.

28 Li M, Yue Q, Liu C, Zheng X, Hong J, Li L *et al.*, Effect of gliadin/glutenin ratio on pasting, thermal, and structural properties of wheat starch. *J Cereal Sci* **93**:102973 (2020). https://doi.org/10.1016/j.jcs.2020.102973.

29 Su H, Tu J, Zheng M, Deng K, Miao S, Zeng S *et al.*, Effects of oligosaccharides on particle structure, pasting and thermal properties of wheat starch granules under different freezing temperatures. *Food Chem* **315**:126209 (2020). https://doi.org/10.1016/j.foodchem.2020.126209.

30 van Soest JJG, Tournois H, de Wit D and Vliegenthart JFG, Short-range structure in (partially) crystalline potato starch determined with attenuated total reflectance Fourier-transform IR spectroscopy. *Carbohydr Res* **279**:201–214 (1995). https://doi.org/10.1016/0008-6215(95)00270-7.

31 López-Barón N, Sagnelli D, Blennow A, Holse M, Gao J, Saaby L *et al.*, Hydrolysed pea proteins mitigate in vitro wheat starch digestibility. *Food Hydrocoll.* **79**:117–126 (2018). https://doi.org/10.1016/j.foodhyd.2017.12.009.

32 Aravind N, Sissons M, Egan N and Fellows C, Effect of insoluble dietary fibre addition on technological, sensory, and structural properties of durum wheat spaghetti. *Food Chem.* **130**:299–309 (2012). https://doi.org/10.1016/j.foodchem.2011.07.042.

33 Ferreira SM, Capriles VD and Conti-Silva AC, Inulin as an ingredient for improvement of glycemic response and sensory acceptance of breakfast cereals. *Food Hydrocoll* **114**:106582 (2021). https://doi.org/10.1016/j.foodhyd.2020.106582.

34 Foschia M, Peressini D, Sensidoni A, Brennan MA and Brennan CS, Synergistic effect of different dietary fibres in pasta on in vitro starch digestion? *Food Chem.* **172**:245–250 (2015). https://doi.org/10.1016/j.foodchem.2014.09.062.

35 Raungrusmee S, Shrestha S, Sadiq MB and Anal AK, Influence of resistant starch, xanthan gum, inulin and defatted rice bran on the physicochemical, functional and sensory properties of low glycemic gluten-free noodles. *LWT* **126**:109279 (2020). https://doi.org/10.1016/j.lwt.2020.109279.

36 Atac LE and Sensoy I, Effects of psyllium and cellulose fibres on thermal, structural, and in vitro digestion behaviour of wheat starch. *Int J Food Sci Technol* **57**:2015–2025 (2022). https://doi.org/10.1111/ijfs.15387.

37 Bilgic H and Sensoy I, Effect of psyllium and cellulose fiber addition on the structure and the starch digestibility of bread and crackers. *Food Struct* **35**:100302 (2022). https://doi.org/10.1016/j.foostr.2022.100302.

38 Sevilmis B and Sensoy I, Effects of psyllium fiber on in vitro digestion and structure of different types of starches. *J Sci Food Agric* **102**:3213–3226 (2022). https://doi.org/10.1002/jsfa.11664.

39 Sozer N, Cicerelli L, Heiniö RL and Poutanen K, Effect of wheat bran addition on invitro starch digestibility, physico-mechanical and sensory properties of biscuits. *J Cereal Sci* **60**:105–113 (2014). https://doi.org/10.1016/j.jcs.2014.01.022.

40 Stewart ML and Zimmer JP, Postprandial glucose and insulin response to a high-fiber muffin top containing resistant starch type 4 in healthy adults: a double-blind, randomized, controlled trial. *Nutrition* **53**:59–63 (2018). https://doi.org/10.1016/j.nut.2018.01.002.

41 Ronda F, Rivero P, Caballero PA and Quilez J, High insoluble fibre content increases in vitro starch digestibility in partially baked breads. *Int J Food Sci Nutr* **63**:971–977 (2012). https://doi.org/10.3109/09637486.2012.690025.

42 Santamaria M, Garzon R and Rosell CM, Impact of starch-hydrocolloid interaction on pasting properties and enzymatic hydrolysis. *Food Hydrocoll* **142**:108764 (2023). https://doi.org/10.1016/j.foodhyd.2023.108764.

43 Santamaria M, Garzon R, Moreira R and Rosell CM, Estimation of viscosity and hydrolysis kinetics of corn starch gels based on microstructural features using a simplified model. *Carbohydr Polym* **273**:118549 (2021). https://doi.org/10.1016/j.carbpol.2021.118549.